Eur. Phys. J. C 37, 141–159 (2004)
Digital Object Identifier (DOI) 10.1140/epjc/s2004-01989-7

THE EUROPEAN PHYSICAL JOURNAL C

Measurement of dijet production at low Q^2 at HERA

The H1 Collaboration

A. Aktas[10], V. Andreev[24], T. Anthonis[4], A. Asmone[31], A. Babaev[23], S. Backovic[35], J. Bähr[35], P. Baranov[24], E. Barrelet[28], W. Bartel[10], S. Baumgartner[36], J. Becker[37], M. Beckingham[21], O. Behnke[13], O. Behrendt[7], A. Belousov[24], Ch. Berger[1], N. Berger[36], T. Berndt[14], J.C. Bizot[26], J. Böhme[10], M.-O. Boenig[7], V. Boudry[27], J. Bracinik[25], W. Braunschweig[1], V. Brisson[26], H.-B. Bröker[2], D.P. Brown[10], D. Bruncko[16], F.W. Büsser[11], A. Bunyatyan[12,34], G. Buschhorn[25], L. Bystritskaya[23], A.J. Campbell[10], S. Caron[1], F. Cassol-Brunner[22], K. Cerny[30], V. Chekelian[25], J. Chýla[29], C. Collard[4], J.G. Contreras[7,41], Y.R. Coppens[3], J.A. Coughlan[5], M.-C. Cousinou[22], B.E. Cox[21], G. Cozzika[9], J. Cvach[29], J.B. Dainton[18], W.D. Dau[15], K. Daum[33,39], B. Delcourt[26], N. Delerue[22], R. Demirchyan[34], A. De Roeck[10,43], K. Desch[11], E.A. De Wolf[4], C. Diaconu[22], J. Dingfelder[13], V. Dodonov[12], J.D. Dowell[3], A. Dubak[25], C. Duprel[2], G. Eckerlin[10], V. Efremenko[23], S. Egli[32], R. Eichler[32], F. Eisele[13], M. Ellerbrock[13], E. Elsen[10], M. Erdmann[10,40,e], W. Erdmann[36], P.J.W. Faulkner[3], L. Favart[4], A. Fedotov[23], R. Felst[10], J. Ferencei[10], M. Fleischer[10], P. Fleischmann[10], Y.H. Fleming[3], G. Flucke[10], G. Flügge[2], A. Fomenko[24], I. Foresti[37], J. Formánek[30], G. Franke[10], G. Frising[1], E. Gabathuler[18], K. Gabathuler[32], J. Garvey[3], J. Gassner[32], J. Gayler[10], R. Gerhards[10,†], C. Gerlich[13], S. Ghazaryan[34], L. Goerlich[6], N. Gogitidze[24], S. Gorbounov[35], C. Grab[36], V. Grabski[34], H. Grässler[2], T. Greenshaw[18], M. Gregori[19], G. Grindhammer[25], D. Haidt[10], L. Hajduk[6], J. Haller[13], G. Heinzelmann[11], R.C.W. Henderson[17], H. Henschel[35], O. Henshaw[3], R. Heremans[4], G. Herrera[7,44], I. Herynek[29], R.-D. Heuer[11], M. Hildebrandt[37], K.H. Hiller[35], J. Hladký[29], P. Höting[2], D. Hoffmann[22], R. Horisberger[32], A. Hovhannisyan[34], M. Ibbotson[21], M. Ismail[21], M. Jacquet[26], L. Janauschek[25], X. Janssen[10], V. Jemanov[11], L. Jönsson[20], C. Johnson[3], D.P. Johnson[4], H. Jung[20,10], D. Kant[19], M. Kapichine[8], M. Karlsson[20], J. Katzy[10], N. Keller[37], J. Kennedy[18], I.R. Kenyon[3], C. Kiesling[25], M. Klein[35], C. Kleinwort[10], T. Kluge[1], G. Knies[10], A. Knutsson[20], B. Koblitz[25], S.D. Kolya[21], V. Korbel[10], P. Kostka[35], R. Koutouev[12], A. Kropivnitskaya[23], J. Kroseberg[37], J. Kückens[10], T. Kuhr[10], M.P.J. Landon[19], W. Lange[35], T. Laštovička[35,30], P. Laycock[18], A. Lebedev[24], B. Leißner[1], R. Lemrani[10], V. Lendermann[10], S. Levonian[10], B. List[36], E. Lobodzinska[35,6], N. Loktionova[24], R. Lopez-Fernandez[10], V. Lubimov[23], H. Lueders[11], S. Lüders[36], D. Lüke[7,10], T. Lux[11], L. Lytkin[12], A. Makankine[8], N. Malden[21], E. Malinovski[24], S. Mangano[36], P. Marage[4], J. Marks[13], R. Marshall[21], M. Martisikova[10], H.-U. Martyn[1], J. Martyniak[6], S.J. Maxfield[18], D. Meer[36], A. Mehta[18], K. Meier[14], A.B. Meyer[11], H. Meyer[33], J. Meyer[10], S. Michine[24], S. Mikocki[6], I. Milcewicz[6], D. Milstead[18], F. Moreau[27], A. Morozov[8], I. Morozov[8], J.V. Morris[5], M. Mozer[13], K. Müller[37], P. Murín[16,42], V. Nagovizin[23], B. Naroska[11], J. Naumann[7], Th. Naumann[35], P.R. Newman[3], C. Niebuhr[10], D. Nikitin[8], G. Nowak[6], M. Nozicka[30], B. Olivier[10], J.E. Olsson[10], G.Ossoskov[8], D. Ozerov[23], C. Pascaud[26], G.D. Patel[18], M. Peez[22], E. Perez[9], A. Perieanu[10], A. Petrukhin[35], D. Pitzl[10], R. Pöschl[10], B. Portheault[26], B. Povh[12], N. Raicevic[35], J. Rauschenberger[11], P. Reimer[29], B. Reisert[25], C. Risler[25], E. Rizvi[3], P. Robmann[37], R. Roosen[4], A. Rostovtsev[23], Z. Rurikova[25], S. Rusakov[24], K. Rybicki[6,†], D.P.C. Sankey[5], E. Sauvan[22], S. Schätzel[13], J. Scheins[10], F.-P. Schilling[10], P. Schleper[10], S. Schmidt[25], S. Schmitt[37], M. Schneider[22], L. Schoeffel[9], A. Schöning[36], V. Schröder[10], H.-C. Schultz-Coulon[7], C. Schwanenberger[10], K. Sedlák[29], F. Sefkow[10], I. Sheviakov[24], L.N. Shtarkov[24], Y. Sirois[27], T. Sloan[17], P. Smirnov[24], Y. Soloviev[24], D. South[21], V. Spaskov[8], A. Specka[27], H. Spitzer[11], R. Stamen[10], B. Stella[31], J. Stiewe[14], I. Strauch[10], U. Straumann[37], M. Taševský[29], G. Thompson[19], P.D. Thompson[3], F. Tomasz[14], D. Traynor[19], P. Truöl[37], G. Tsipolitis[10,38], I. Tsurin[35], J. Turnau[6], E. Tzamariudaki[25], A. Uraev[23], M. Urban[37], A. Usik[24], S. Valkár[30], A. Valkárová[30], C. Vallée[22], P. Van Mechelen[4], A. Vargas Trevino[7], S. Vassiliev[8], Y. Vazdik[24], C. Veelken[18], A. Vest[1], A. Vichnevski[8], S. Vinokurova[10], V. Volchinski[34], K. Wacker[7], J. Wagner[10], B. Waugh[21], G. Weber[11], R. Weber[36], D. Wegener[7], C. Werner[13], N. Werner[37], M. Wessels[1], B. Wessling[11], M. Winde[35], G.-G. Winter[10], Ch. Wissing[7], E.-E. Woehrling[3], E. Wünsch[10], W. Yan[10], J. Žáček[30], J. Zálešák[30], Z. Zhang[26], A. Zhokin[23], H. Zohrabyan[34], F. Zomer[26]

[1] I. Physikalisches Institut der RWTH, Aachen, Germany[a]
[2] III. Physikalisches Institut der RWTH, Aachen, Germany[a]
[3] School of Physics and Space Research, University of Birmingham, Birmingham, UK[b]
[4] Inter-University Institute for High Energies ULB-VUB, Brussels; Universiteit Antwerpen (UIA), Antwerpen; Belgium[c]
[5] Rutherford Appleton Laboratory, Chilton, Didcot, UK[b]
[6] Institute for Nuclear Physics, Cracow, Poland[d]
[7] Institut für Physik, Universität Dortmund, Dortmund, Germany[a]
[8] Joint Institute for Nuclear Research, Dubna, Russia

[9] CEA, DSM/DAPNIA, CE-Saclay, Gif-sur-Yvette, France
[10] DESY, Hamburg, Germany
[11] Institut für Experimentalphysik, Universität Hamburg, Germany[a]
[12] Max-Planck-Institut für Kernphysik, Heidelberg, Germany
[13] Physikalisches Institut, Universität Heidelberg, Germany[a]
[14] Kirchhoff-Institut für Physik, Universität Heidelberg, Germany[a]
[15] Institut für experimentelle und Angewandte Physik, Universität Kiel, Kiel, Germany
[16] Institute of Experimental Physics, Slovak Academy of Sciences, Košice, Slovak Republic[e,f]
[17] School of Physics and Chemistry, University of Lancaster, Lancaster, UK[b]
[18] Department of Physics, University of Liverpool, Liverpool, UK[b]
[19] Queen Mary and Westfield College, London, UK[b]
[20] Physics Department, University of Lund, Lund, Sweden[g]
[21] Physics Department, University of Manchester, Manchester, UK[b]
[22] CPPM, CNRS/IN2P3 - Univ Mediterranee, Marseille - France
[23] Institute for Theoretical and Experimental Physics, Moscow, Russia[l]
[24] Lebedev Physical Institute, Moscow, Russia[e]
[25] Max-Planck-Institut für Physik, München, Germany
[26] LAL, Université de Paris-Sud, IN2P3-CNRS, Orsay, France
[27] LLR, Ecole Polytechnique, IN2P3-CNRS, Palaiseau, France
[28] LPNHE, Universités Paris VI and VII, IN2P3-CNRS, Paris, France
[29] Institute of Physics, Academy of Sciences of the Czech Republic, Praha, Czech Republic[e,i]
[30] Faculty of Mathematics and Physics, Charles University, Praha, Czech Republic[e,i]
[31] Dipartimento di Fisica Università di Roma Tre and INFN Roma 3, Roma, Italy
[32] Paul Scherrer Institut, Villigen, Switzerland
[33] Fachbereich Physik, Bergische Universität Gesamthochschule Wuppertal, Germany
[34] Yerevan Physics Institute, Yerevan, Armenia
[35] DESY, Zeuthen, Germany
[36] Institut für Teilchenphysik, ETH, Zürich, Switzerland[j]
[37] Physik-Institut der Universität Zürich, Zürich, Switzerland[j]
[38] Also at Physics Department, National Technical University, Zografou Campus, GR-15773 Athens, Greece
[39] Also at Rechenzentrum, Bergische Universität Gesamthochschule Wuppertal, Germany
[40] Also at Institut für Experimentelle Kernphysik, Universität Karlsruhe, Karlsruhe, Germany
[41] Also at Dept. Fis. Ap. CINVESTAV, Mérida, Yucatán, México[k]
[42] Also at University of P.J. Šafárik, Košice, Slovak Republic
[43] Also at CERN, Geneva, Switzerland
[44] Also at Dept. Fis. CINVESTAV, México City, México[k]
[†] Deceased

Received: 13 January 2004 / Revised version: 21 July 2004 /
Published online: 18 August 2004 – © Springer-Verlag / Società Italiana di Fisica 2004

Abstract. Triple differential dijet cross sections in $e^{\pm}p$ interactions are presented in the region of photon virtualities $2 < Q^2 < 80\,\mathrm{GeV}^2$, inelasticities $0.1 < y < 0.85$, jet transverse energies $E^*_{T\,1} > 7\,\mathrm{GeV}$, $E^*_{T\,2} > 5\,\mathrm{GeV}$, and pseudorapidities $-2.5 < \eta^*_1, \eta^*_2 < 0$. The measurements are made in the $\gamma^* p$ centre-of-mass frame, using an integrated luminosity of 57 pb^{-1}. The data are compared with NLO QCD calculations and LO Monte Carlo programs with and without a resolved virtual photon contribution. NLO QCD calculations fail to describe the region of low Q^2 and low jet transverse energies, in contrast to a LO Monte Carlo generator which includes direct and resolved photon interactions with both transversely and longitudinally polarised photons. Initial and final state parton showers are tested as a mechanism for including higher order QCD effects in low E_T jet production.

[a] Supported by the Bundesministerium für Bildung und Forschung, FRG, under contract numbers 05 H1 1GUA /1, 05 H1 1PAA /1, 05 H1 1PAB /9, 05 H1 1PEA /6, 05 H1 1VHA /7 and 05 H1 1VHB /5
[b] Supported by the UK Particle Physics and Astronomy Research Council, and formerly by the UK Science and Engineering Research Council
[c] Supported by FNRS-FWO-Vlaanderen, IISN-IIKW and IWT
[d] Partially Supported by the Polish State Committee for Scientific Research, SPUB/DESY/P003/DZ 118/2003/2005
[e] Supported by the Deutsche Forschungsgemeinschaft
[f] Supported by VEGA SR grant no. 2/1169/2001
[g] Supported by the Swedish Natural Science Research Council
[i] Supported by the Ministry of Education of the Czech Republic under the projects INGO-LA116/2000 and LN00A006, by GAUK grant no 173/2000
[j] Supported by the Swiss National Science Foundation
[k] Supported by CONACyT

1 Introduction

Jet cross sections in electron-proton collisions are successfully described by next-to-leading order (NLO) QCD calculations in most of the HERA kinematic range [1–6]. However, regions of phase space have previously been observed for which NLO predictions do not reproduce the data satisfactorily and leading order (LO) Monte Carlo simulations with different approaches to modelling higher order QCD effects are often more successful [3–9].

At HERA, a photon coupling to the incoming electron interacts with a parton from the proton. The measurement of dijet production is particularly suitable for the investigation of effects related to photon structure, which have been studied during the last two decades in e^+e^- and ep collisions [10,11]. In the "photoproduction" region of ep interactions, i.e. for $Q^2 \ll \Lambda^2_{\rm QCD}$, the interaction can be described by the sum of two contributions. In the *direct photon* process, the photon interacts as a whole with a parton from the proton, whereas in the *resolved photon* process, it behaves as a source of partons, which interact with partons from the proton.

As the virtuality of the photon increases, the role of photon structure gradually changes. Whereas for quasi-real photons it is an indispensable theoretical tool, for $Q^2 \gg \Lambda^2_{\rm QCD}$ the concept of a resolved photon is usually discarded and the data are analysed within the framework of perturbative calculations of direct photon processes. However, it has been argued [12–15] that the concept of the resolved photon is very useful phenomenologically for arbitrary Q^2, provided the photon virtuality remains much smaller than some measure of the hardness of the process in which the photon participates. In our case this is satisfied for $Q^2 \ll E_T^2$, where E_T denotes the jet transverse energy. Experimental evidence for the resolved virtual photon contribution has been found in a number of publications [7,16,17].

In this paper, new data on dijet production, obtained with the H1 detector in the kinematic region of low to moderate photon virtualities $2 < Q^2 < 80\,\mathrm{GeV}^2$, are presented as triple differential distributions in Q^2, the inelasticity y and variables characterising the final state jets. The data are compared with predictions within several theoretical approaches, differing in the way QCD effects are taken into account beyond LO, in order to identify which of them are successful in which regions. In doing that we use NLO calculations (i.e. including terms up to order $\alpha\alpha_s^2$) as well as LO calculations supplemented with parton showers, which take into account leading logarithmic contributions to all orders. The effects of resolved virtual photons are studied for both transverse and longitudinal photon polarisations.

The paper is organised as follows. After a review of various theoretical approaches to the description of interactions of virtual photons in Sect. 2, a brief description of the detector is given in Sect. 3. The data sample and event selection are specified in Sect. 4. Background subtractions, detector corrections and estimates of the measurement uncertainties are discussed in Sect. 5. The results are presented and discussed in Sect. 6.

[1] Partially Supported by Russian Foundation for Basic Research, grant no. 00-15-96584

2 Dynamics of hard processes in ep collisions

2.1 The DGLAP approach

The DGLAP approach uses parton distribution functions (PDFs) of the proton extracted from analyses of data on hard scattering processes. These PDFs depend on the factorisation scale μ_f, satisfy the DGLAP [18] evolution equations, and are sometimes called "integrated" to emphasise the fact that their definition involves an integral over the virtualities of partons up to μ_f^2.

In this approach, the cross section for dijet production in our kinematic region is given by the direct photon contribution, illustrated in Fig. 1a,b, and expressed as

$$\sigma^{\rm DIR} \sim \sum_j D_{j/p} \otimes \sigma_{ej}\,,$$
$$\sigma_{ej} = c_{ej}^{(1)}\alpha_s + c_{ej}^{(2)}\alpha_s^2 + \cdots\,, \qquad (1)$$

where σ_{ej} denotes the cross section for a collision between the incoming electron and a parton j from the proton, $c_{ej}^{(1)}, c_{ej}^{(2)}, \cdots$ are coefficients of an expansion of σ_{ej} in powers of α_s and $D_{j/p}$ denotes the PDF of the proton. The term $c_{ej}^{(1)}\alpha_s$ defines the LO cross section, whilst $c_{ej}^{(1)}\alpha_s + c_{ej}^{(2)}\alpha_s^2$ defines the NLO cross section.

Recent analyses [3,7,16] of dijet cross sections in the region $\Lambda^2_{\rm QCD} < Q^2 < E_T^2$ have convincingly shown that the LO direct photon contribution lies significantly below the data. The NLO calculations, involving diagrams such as that shown in Fig. 1b, bring the theoretical prediction closer to the data [3]. A recent H1 analysis [4] indicates that even the NLO calculations do not completely describe inclusive jet production at low Q^2 in part of the phase space. Large values of the NLO corrections, i.e. the ratio of NLO to LO predictions for the cross sections, and high sensitivity of the predicted jet cross sections to variations of the factorisation and renormalisation scales, strongly suggest the need for higher order (i.e. $c_{ej}^{(3)}, c_{ej}^{(4)}, \cdots$) terms in (1). In the absence of a full calculation beyond NLO, some approximate procedure for resummation of the dominant higher order terms in (1) can be constructed. This procedure is based on the fact that in part of the phase space, the upper vertex of the diagram in Fig. 1b can be viewed as the splitting of the photon into a $q\bar{q}$ pair. Taking into account subsequent emissions of partons from this $q\bar{q}$ pair, these terms can be resummed into the PDF of the photon[1], D_{i/γ_T^*}, as is done for instance in [12], and D_{i/γ_L^*}

[1] This resummation actually yields the point-like (sometimes called "anomalous") parts of the photon PDF, which dominate in the kinematic region studied in this paper, where the hadronic (sometimes called "VMD") parts of the photon PDF are negligible.

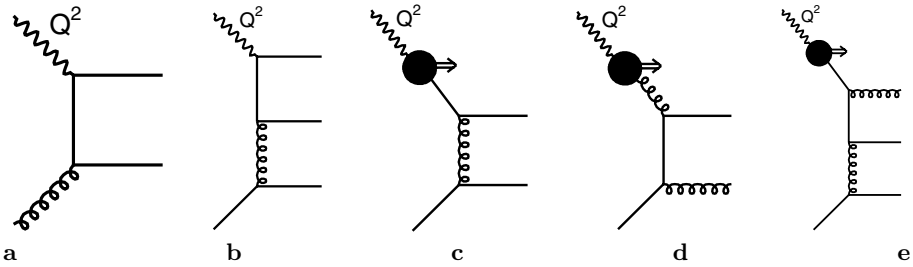

Fig. 1. Examples of diagrams for the production of at least two jets (incoming electrons and protons not shown): LO (**a**) and NLO (**b**) direct photon interactions; LO resolved photon interactions involving a quark (**c**) or a gluon (**d**) from the photon; NLO resolved photon process (**e**)

in [19], where γ_T^* denotes the transversely and γ_L^* the longitudinally polarised virtual photon [20,21].

Consequently, one can calculate the resolved photon contribution to the dijet cross section, corresponding to the graphs shown in Fig. 1c,d,e, as

$$\sigma^{\mathrm{RES}} \sim \sum_{k=T,L} f_k \otimes \sum_{i,j} D_{i/\gamma_k^*} \otimes D_{j/p} \otimes \sigma_{ij}\,,$$
$$\sigma_{ij} = c_{ij}^{(1)}\alpha_s^2 + c_{ij}^{(2)}\alpha_s^3 + \cdots\,, \qquad (2)$$

where i, j run over all partons in the photon and proton respectively, σ_{ij} is the partonic cross section, $c_{ij}^{(1)}\alpha_s^2$ defines the LO resolved photon cross section, $c_{ij}^{(1)}\alpha_s^2 + c_{ij}^{(2)}\alpha_s^3$ the NLO resolved photon cross section and f_T, f_L denote the fluxes of transversely and longitudinally polarised virtual photons, respectively:

$$f_T(y,Q^2) = \frac{\alpha}{2\pi}\left[\frac{2(1-y)+y^2}{y}\frac{1}{Q^2} - \frac{2m_e^2 y}{Q^4}\right], \qquad (3)$$

$$f_L(y,Q^2) = \frac{\alpha}{2\pi}\left[\frac{2(1-y)}{y}\frac{1}{Q^2}\right]. \qquad (4)$$

The final dijet cross section is then given by the sum[2] of σ^{DIR} and σ^{RES}.

There is an interesting connection between the direct and resolved photon contributions. In a large part of the phase space, the NLO direct calculations (Fig. 1b) can be reasonably well approximated by the sum of the LO direct (Fig. 1a) and LO resolved (Fig. 1c) photon contributions, provided the simplest expression, namely that given by the pure QED splitting of the photon into a $q\overline{q}$ pair, is used for the photon PDF [22]. In our kinematic region and for quark masses $m_q^2 \ll Q^2$, the pure QED photon PDFs have the form

$$D^{\mathrm{QED}}_{q_i/\gamma_T^*}(x_\gamma, Q^2, E_T^2)$$
$$= \frac{\alpha}{2\pi} 3e_i^2 \left(x_\gamma^2 + (1-x_\gamma)^2\right) \ln\frac{E_T^2}{x_\gamma Q^2}, \qquad (5)$$

$$D^{\mathrm{QED}}_{q_i/\gamma_L^*}(x_\gamma, Q^2, E_T^2)$$
$$= \frac{\alpha}{2\pi} 3e_i^2 4x_\gamma(1-x_\gamma)\left(1 - \frac{x_\gamma Q^2}{E_T^2}\right), \qquad (6)$$

$$D^{\mathrm{QED}}_{g/\gamma^*_{T,L}}(x_\gamma, Q^2, E_T^2) = 0. \qquad (7)$$

In (5)–(7), e_i denotes the electric charge of the quark q_i and x_γ denotes the four-momentum fraction of the photon carried by the quark. The full expressions for the distribution functions from (5)–(7), containing the exact Q^2 dependence with the correct threshold behaviour for $Q^2/m_q^2 \to 0$, can be found in [15].

2.2 The CCFM approach

The CCFM [23] approach uses the more general concept of an "unintegrated" PDF of the proton in the region of small Bjorken-x. The virtualities and transverse momenta of the propagating partons are no longer ordered, as is the case for DGLAP evolution. Instead, an angular ordering of emissions is introduced in order to correctly treat gluon coherence effects [23]. Similarly to the case of the DGLAP scheme in (1), the cross section can be factorised into a partonic cross section and universal parton distribution functions according to [24]

$$\sigma^{k_T\ \mathrm{FACTORISATION}} = \sum_j \int \frac{dz}{z}\, d^2k_T\, \hat{\sigma}_{ej}(\frac{x}{z}, k_T^2)\; A_{j/p}(x, k_T^2, \hat{\mu}_f^2)\;, \qquad (8)$$

where the partonic cross sections $\hat{\sigma}_{ej}$ have to be taken off-shell (i.e. dependent on the parton transverse momentum, k_T), $\hat{\mu}_f$ is the factorisation scale related to the maximum angle allowed in the evolution, and the unintegrated parton distributions, $A_{j/p}(x, k_T^2, \hat{\mu}_f^2)$, depend on an additional variable, the k_T of parton j.

The CCFM evolution scheme provides a framework for the implementation of k_T-unordered initial state QCD cascades. The partons with the largest k_T may come from any emission in the proton cascade, not necessarily from the hard subprocess as in the DGLAP framework. This can lead to events which have a similar topology to that

[2] Care must be taken when adding the contribution of the LO resolved photon diagram (Fig. 1c) to the NLO direct photon term (Fig. 1b). To avoid double counting, the so called photon splitting term must be subtracted from the NLO direct photon contribution of the diagram in Fig. 1b. In this paper the term "direct contribution" denotes the direct photon contribution before the subtraction of the splitting term.

of the resolved photon interaction in the DGLAP approximation [25], where hard partons are accompanied by softer partons from the photon remnant.

The mean value of the proton momentum fraction x_p, appearing as an argument of the unintegrated PDFs, is $\langle x_p \rangle \simeq 0.03$ in our kinematic region. Even though this value may not be small enough for the CCFM approach to be superior to that based on the standard integrated PDF and DGLAP evolution equations, it is interesting to compare the CCFM predictions with the data. Recently, such comparisons became possible using the CASCADE Monte Carlo (MC) generator.

2.3 Programs for dijet calculations

Several MC programs can be used for predictions of dijet cross sections, as discussed below.

HERWIG [26] is a general purpose LO MC event generator, applicable to a wide range of hard processes and collisions, including direct and resolved photon interactions in the region of moderate Q^2. It is based on LO cross sections in the DGLAP approach, interfaced to leading-logarithm parton showers. Hadronisation is done via the decay of colourless clusters, formed during the hard scattering and parton shower stages. HERWIG is also able to model additional soft remnant-remnant interactions (the "soft underlying event"), accompanying the hard scattering process. The probability that a resolved photon event contains soft underlying activity has been adjusted as in [16] so that the energy flow in and around the jets is well described. Only transversely polarised photons are included for resolved photon interactions in the default version of HERWIG. To investigate the contributions of resolved longitudinal photons, we have modified HERWIG by adding the option of simulating the flux in (4). Similarly the QED PDFs of the photon from (5–7) have been implemented in HERWIG in order to study the differences between the results obtained with the pure QED and the QCD-improved photon PDFs. The scales μ_r and μ_f are set to a combination of Mandelstam variables [26], which roughly corresponds to $1.1p_T$, where p_T denotes transverse momentum of the outgoing parton from the hard interaction.

RAPGAP [27] combines standard LO hard scattering matrix elements in the DGLAP approach with parton showers and LUND string fragmentation, using JETSET [28,29]. Only the transverse virtual photon is considered in resolved photon processes. Soft underlying interactions are not modelled.

DISENT [30] is a NLO DGLAP program for calculating dijet cross sections at the parton level. It is based on the dipole subtraction method [31] to regularise soft and collinear divergences. The factorisation scale, μ_f, was set to $\langle E_T \rangle = 9\,\text{GeV}$, since the program does not allow the user to set $\mu_f = E_T$ for each point in phase space. In our kinematic region, the difference between the results obtained with $\mu_f = E_T$ and $\mu_f = \langle E_T \rangle$, tested using JETVIP, is very small. DISENT does not include resolved photon interactions.

JETVIP [32, 33] is a NLO DGLAP parton level program which calculates both direct and resolved photon contributions. It is based on the phase space slicing method. We have performed systematic investigations of the stability of JETVIP calculations with respect to variations of the slicing parameter y_c [22]. The direct contribution in our kinematic region is independent of y_c to within 5% over the recommended range of its values $10^{-4} \leq y_c \leq 10^{-2}$. The situation changes in the case of the NLO resolved photon contribution, for which the dependence on the y_c parameter is significantly larger. The sum of NLO direct and NLO resolved JETVIP predictions varies by 30% in some bins for the recommended range of y_c . We set $y_c = 0.003$ in all JETVIP calculations, since the predictions are most stable around this value.

Table 1. Parameters of the MC programs. The variable p_T denotes the transverse momentum of the parton with mass m_q outgoing from the hard interaction and $E^*_{T\,1}$ is the energy of the jet with the highest transverse energy. The parameter PRSOF specifies the fraction of resolved photon events with soft underlying activity

Parameters	HERWIG	RAPGAP	CASCADE	DISENT	JETVIP
Version	6.4	2.8	1.2	—	2.1
Proton PDF	CTEQ5L [36]	CTEQ5L	J2003 (set 1) [37]	CTEQ6M	CTEQ6M
Photon PDF	SAS1D [12]; [19] for γ^*_L	SAS1D	—	—	SAS1D
Formula for α_s	one-loop	one-loop	one-loop	two-loop	two-loop
Active flavours	5	5	4	5	5
PRSOF	10%	—	—	—	—
μ_r	$\sim 1.1p_T$	$\sqrt{(p_T^2 + m_q^2)}$	$\sqrt{(p_T^2 + m_q^2)}$	$E^*_{T\,1}$	$E^*_{T\,1}$
μ_f	$\sim 1.1p_T$	$\sqrt{(p_T^2 + m_q^2)}$	given by ang. ordering	9 GeV	$E^*_{T\,1}$
Hadronisation mechanism	Cluster model	LUND string fragmentation	LUND string fragmentation	—	—

We have observed non-negligible differences between the differential dijet cross section obtained with DISENT and the direct contribution from JETVIP (see Sect. 6.1). We have checked that this discrepancy is not caused by different input parameters or kinematic cuts, as the leading order, i.e. $O(\alpha\alpha_s)$, contributions agree perfectly. We therefore test both programs in our analysis.

CASCADE [34,35] is a LO MC event generator. It uses unintegrated gluon distribution functions of the proton, satisfying the CCFM equation, and correspondingly produces a k_T unordered initial state parton shower. The LUND string model is used for fragmentation.

The parameter settings of all MC programs and NLO calculations are summarised in Table 1.

In the NLO calculations, JETVIP and DISENT, the massless partons entering the hard process are taken to be exactly collinear with the beam particles. On the other hand, the Monte Carlo generators HERWIG, RAPGAP and CASCADE generate initial state QCD parton showers, which influence the four-momenta of partons entering the hard process by generating the appropriate transverse momentum. Both initial and final state parton showers also provide more partons in the final state. These effects tend to produce more low E_T jets in the LO models than in the NLO calculations.

2.4 Hadronisation corrections

The MC event generators have a clear advantage over the parton level calculations in incorporating hadronisation effects. In order to estimate the hadronisation corrections to the NLO calculations, we use two different Monte Carlo models, HERWIG and LEPTO [38], and divide the cross sections obtained from these models for the complete hadronic final state by the cross sections predicted from the partonic final state after the initial and final state QCD parton showers. The hadronisation corrections determined by HERWIG also include corrections for the soft underlying event. The average values of the corrections obtained with HERWIG and LEPTO are applied to the NLO calculations as bin-by-bin correction factors and half the difference between the corrections obtained with the two models is taken as a hadronisation uncertainty in the NLO predictions. The hadronisation effects usually do not change the NLO predictions by more than 5%, with the exception of the cross section differential in x_γ, for which the corrections change the cross section by up to 15%.

3 Detector description

A detailed description of the H1 detector can be found elsewhere [39] and only the components relevant for this analysis are described here.

The H1 central tracking system is mounted concentrically around the beam-line and covers polar angles[3] $20^\circ < \theta < 160^\circ$. The transverse momenta and charges of charged particles are measured by two coaxial cylindrical drift chambers [40]. Two drift chambers which provide accurate measurements of the z coordinate of charged tracks and two multi-wire proportional chambers which trigger on these tracks are placed on either side of the inner main drift chamber.

The tracking system is surrounded by a finely segmented Liquid Argon Calorimeter [41], which covers the range of polar angles $4^\circ < \theta < 154^\circ$ and the full range in azimuth. It consists of an electromagnetic section with lead absorbers, 20–30 radiation lengths in depth, and a hadronic section with steel absorbers. The total depth of the calorimeter ranges from 4.5 to 8 hadronic interaction lengths. The energy resolution obtained from test beam measurements [42] is $\sigma(E)/E \approx 0.11/\sqrt{E}$ for electrons and $\sigma(E)/E \approx 0.5/\sqrt{E}$ for pions, with E in GeV. The absolute energy scale for hadrons is known for this analysis to a precision of 4%. A uniform axial magnetic field of 1.15 T is provided by a superconducting coil, which surrounds the calorimeter.

The polar angle region $153^\circ < \theta < 177.8^\circ$ is covered by the SPACAL [43], a lead/scintillating fibre calorimeter with electromagnetic and hadronic sections. The energy resolution of the electromagnetic section is determined to be $0.07/\sqrt{E} \oplus 0.01$ (E in GeV) [44]. Both calorimeter sections have a time resolution better than 1 ns. The SPACAL is used both to trigger on the scattered electron[4] and to measure its energy. In front of the SPACAL, an eight layer drift chamber, BDC [45], covers the polar angle region $151^\circ < \theta < 177.5^\circ$. It is used to suppress background from neutral particles faking the scattered electron and, together with the vertex obtained from the central drift chambers, to measure the scattered electron polar angle θ.

4 Data samples and event selection

The present analysis is based on data taken in the years 1999 and 2000, when electrons with an energy of 27.55 GeV collided with protons with an energy of 920 GeV. The data correspond to an integrated luminosity of 57 pb^{-1}. 83% of the data sample corresponds to e^+p collisions, the remainder to e^-p interactions.

The kinematic region covered by the analysis is defined by cuts on the photon virtuality, Q^2, the inelasticity, y, and by cuts on the hadronic final state. We require

$$2 < Q^2 < 80 \text{ GeV}^2,$$

$$0.1 < y < 0.85.$$

[3] The z axis of the right-handed coordinate system used by H1 is defined to lie along the direction of the proton beam with the origin at the nominal ep interaction vertex.

[4] In the following, the notation "electrons" stands for both positrons and electrons.

The variables Q^2 and y were determined using the scattered electron energy and polar angle [16].

The final state has to contain at least two jets. Jets are found using the longitudinally invariant k_t jet algorithm [46] applied to hadronic final state "combined objects", boosted into the photon-proton centre-of-mass frame. The combined objects are constructed from tracks in the central track chambers and clusters in the SPACAL and LAr calorimeters in a procedure that avoids double counting [47]. The jet transverse energies, E_T^*, and pseudorapidities, η^*, are calculated relative to the $\gamma^* p$ collision axis in the $\gamma^* p$ centre-of-mass frame[5]. The jets are ordered according to their transverse energy, with jet 1 being the highest E_T^* jet.

The two jets with the highest transverse energies (leading jets) are required to have

$$E_{T\,1}^* > 7 \text{ GeV}, \quad E_{T\,2}^* > 5 \text{ GeV},$$

$$-2.5 < \eta_1^* < 0, \quad -2.5 < \eta_2^* < 0.$$

The asymmetric E_T^* cuts avoid regions of instability in the NLO calculations [48, 49].

The reconstructed event vertex has to be within ± 35 cm of the nominal interaction point, which substantially reduces contributions from beam induced background. To remove background from photoproduction processes, a cut $45 < \sum_i (E_i - p_{z,i}) < 75$ GeV is applied, where the sum runs over all particles in the final state including the scattered electron. In total 105 658 events satisfied the selection criteria.

It is convenient to describe dijet events by means of the variable x_γ^{jets}, defined as

$$x_\gamma^{\text{jets}} = \frac{\sum\limits_{j=1,2} (E_j^* - p_{z,j}^*)}{\sum\limits_{\text{hadrons}} (E^* - p_z^*)}\,, \tag{9}$$

where the sum in the numerator runs over the two leading jets and the sum in the denominator includes the full hadronic final state. Neglecting the masses of the partons and beam particles, the variable x_γ^{jets} represents a hadron level estimate of the fraction of the photon four-momentum carried by the parton involved in the hard scattering.

5 Analysis procedure

The data were corrected for initial and final state QED radiation effects using samples of RAPGAP events for direct photon interactions with and without QED radiation, processed through the full detector simulation and fulfilling all the cuts described in the previous section. The effects of trigger inefficiencies, limited detector acceptance and resolution were corrected for using an iterative Bayesian unfolding technique [50], which was applied to events generated by HERWIG and RAPGAP. For this purpose, 4 million events from each generator were passed through the full simulation of the H1 detector and the same chain of reconstruction and analysis procedure as for the data.

The binning for the final results was chosen such that the bin width is always larger than the resolution of the given quantity[6]. The iterative Bayesian procedure converged in all bins of the measured quantities [22]. After unfolding, the correlations between neighbouring bins in the unfolded distributions were always less than 60%. The correction factors from the unfolding procedure were cross-checked with a bin-by-bin correction method, performed using the same simulated MC samples, and agreement was found to within 5%.

In all of the distributions studied, the presented cross sections are taken as averages of the cross sections obtained when correcting for detector effects using HERWIG and RAPGAP, since the description from the two models of the uncorrected distributions are of similar quality.

The background in the event sample from photoproduction events, in which a hadron in the SPACAL is misidentified as the electron candidate, was estimated using PYTHIA [29] and PHOJET [51] MC samples of photoproduction events. This background is negligible for most of the bins and reaches 4% at the highest y.

The systematic errors are added in quadrature. They are listed below in order of their size:

- *Model dependence.* The systematic error from the model dependence of the acceptance corrections, including that due to the soft underlying event, is taken as half of the difference between the results when unfolded with RAPGAP and with HERWIG. This leads to an error of 5–10% on average, reaching 20% in the most extreme case.
- *Energy calibration of the calorimeters.* Varying the overall hadronic energy scale of the LAr calorimeter by 4%, the hadronic energy scale of the SPACAL by 7% and the electromagnetic energy scale of the SPACAL by 1% leads to systematic shifts of the results by typically 10%, 2% and 4%, respectively.
- *Scattered electron angle.* The polar angle of the scattered electron is measured with a precision of 1 mrad, which leads to a 3% (1%) systematic uncertainty in the lowest (highest) Q^2 region.
- *Trigger efficiency.* The uncertainty in the trigger efficiency leads to a 3% uncertainty in the measurement.
- *QED radiative corrections.* 2% is taken as the systematic error in all bins [22].
- *Stability of the Bayesian unfolding procedure.* By varying the number of iterations used in the unfolding procedure, the uncertainty due to the unfolding instability

[5] The pseudorapidity is defined by $\eta^* \equiv -\ln(\tan\theta^*/2)$, where θ^* is the polar angle of the jet axis with respect to the $\gamma^* p$ collision axis. Negative values of η^* correspond to the photon fragmentation region. The pseudorapidity in the photon-proton centre-of-mass frame is shifted on average by -2.3 units with respect to the pseudorapidity in the laboratory frame.

[6] The experimental resolutions on the kinematic variables studied are typically $\delta(Q^2)/Q^2 \sim 0.03$, $\delta(y) \sim 0.015$, $\delta\,(x_\gamma^{\text{jets}}) \sim 0.08$, $\delta\,(E_T^*)\,/\,E_T^* \sim 0.15$ and $\delta\,(\eta^*) \sim 0.12$.

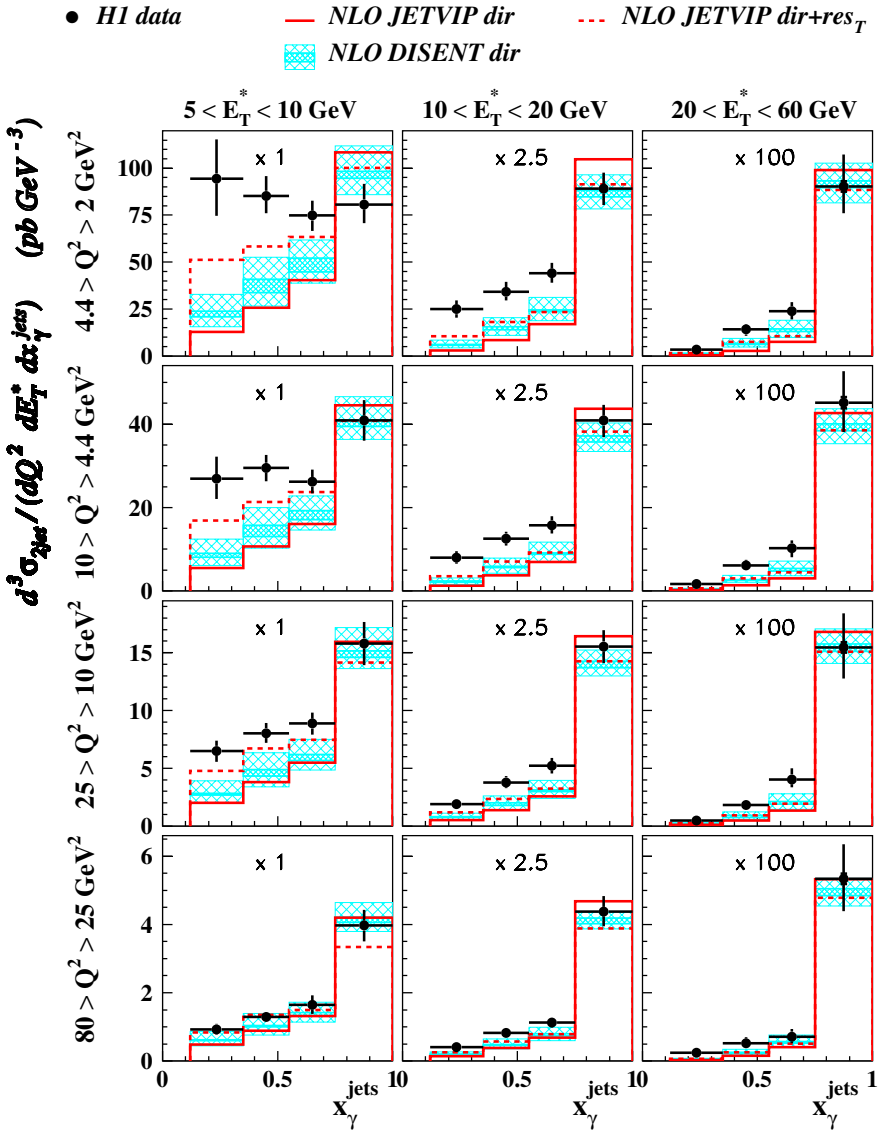

Fig. 2. Triple differential dijet cross section, $\mathrm{d}^3\sigma_{2\mathrm{jet}}/\mathrm{d}Q^2\mathrm{d}E_T^*\,\mathrm{d}x_\gamma^{\mathrm{jets}}$, with asymmetric E_T^* cuts (see text). The inner error bars on the data points show the statistical error, the outer error bars show the quadratic sum of systematic and statistical errors. Also shown are NLO direct photon calculations using DISENT (hatched area) and JETVIP (full line), as well as the sum of NLO direct and NLO resolved photon contributions of JETVIP (dashed line). All calculations are corrected for hadronisation effects. The inner hatched area illustrates the uncertainty due to the hadronisation corrections, the outer hatched area shows the quadratic sum of the errors from hadronisation and the scale uncertainty (shown only for DISENT). The scale factors applied to the cross sections are given

is estimated to be typically less than 2% and at most 5%.

– *Photoproduction background.* The photoproduction background is subtracted statistically and half of the subtracted background is taken as the systematic uncertainty.
– *Precision of the luminosity measurement.* The normalisation uncertainty due to the luminosity measurement is 1.5%.

6 Results

Differential cross sections for the kinematic region defined in Sect. 4 are discussed in the following sections and presented in Tables 2–5.

6.1 Comparison with NLO calculations

The triple differential dijet cross section is presented as a function of x_γ^{jets} in different bins of Q^2 and E_T^* in Fig. 2. The variable E_T^* denotes the transverse energies of the jets with the highest and second highest E_T^* measured in the photon-proton centre-of-mass frame, so that each event contributes twice to the distributions, not necessarily in the same bin. The data are compared with the NLO direct photon calculations[7] performed with DISENT and JETVIP. The uncertainties from variations of the factorisation and renormalisation scales in the interval $\mu/2$ to 2μ, as well as from hadronisation corrections, are illustrated. The scale uncertainties are typically around 20%. Those from hadronisation are at the 7% level. We have also investigated the uncertainties due to variations of the proton PDF, using the prescription of [52]. The typical uncertainties are below 4% (not shown). Figure 2 demonstrates that the NLO direct photon calculations describe the data in the region of high x_γ^{jets}, where direct photon interactions dominate. For $x_\gamma^{\mathrm{jets}} < 0.75$, the description is nowhere perfect, indicating the need for orders beyond

[7] The resolved photon prediction of JETVIP, also shown in Fig. 2, is discussed in Sect. 6.2.

Table 2. Triple differential dijet cross section, $\mathrm{d}^3\sigma_{2\mathrm{jet}}/\mathrm{d}Q^2\mathrm{d}E_T^*\,\mathrm{d}x_\gamma^{\mathrm{jets}}$. The cross section is given together with the statistical and systematic uncertainties. The correction factors for hadronisation effects applied to the NLO QCD predictions are also given

Q^2 (GeV^2)	E_T^* (GeV)	x_γ	$\mathrm{d}^3\sigma_{2\mathrm{jet}}/\mathrm{d}Q^2\mathrm{d}E_T^*\,\mathrm{d}x_\gamma^{\mathrm{jets}}$ (pb/GeV^3)	δ_{stat} (pb/GeV^3)	δ_{syst} (pb/GeV^3)	hadr. corr.
2.0 – 4.4	5 – 10	0.12 – 0.35	94	1	20	0.78
		0.35 – 0.55	85.3	1.0	9.9	0.81
		0.55 – 0.75	74.8	0.9	7.9	1.17
		0.75 – 1.00	81	1	10	1.04
	10 – 20	0.12 – 0.35	10.0	0.2	1.8	0.87
		0.35 – 0.55	13.6	0.2	2.0	0.88
		0.55 – 0.75	17.6	0.2	2.1	1.03
		0.75 – 1.00	35.6	0.4	3.4	1.01
	20 – 60	0.12 – 0.35	0.033	0.004	0.010	0.81
		0.35 – 0.55	0.141	0.010	0.029	0.93
		0.55 – 0.75	0.239	0.012	0.045	0.94
		0.75 – 1.00	0.90	0.03	0.15	0.98
4.4 – 10	5 – 10	0.12 – 0.35	26.9	0.3	5.1	0.80
		0.35 – 0.55	29.5	0.3	3.2	0.82
		0.55 – 0.75	26.2	0.2	2.8	1.19
		0.75 – 1.00	40.9	0.4	4.8	1.05
	10 – 20	0.12 – 0.35	3.20	0.06	0.60	0.86
		0.35 – 0.55	5.03	0.07	0.66	0.90
		0.55 – 0.75	6.31	0.07	0.84	1.02
		0.75 – 1.00	16.3	0.2	1.5	1.02
	20 – 60	0.12 – 0.35	0.0169	0.0022	0.0050	0.88
		0.35 – 0.55	0.061	0.004	0.012	0.97
		0.55 – 0.75	0.103	0.006	0.019	0.89
		0.75 – 1.00	0.451	0.014	0.072	0.98
10 – 25	5 – 10	0.12 – 0.35	6.50	0.09	0.91	0.83
		0.35 – 0.55	8.03	0.08	0.86	0.85
		0.55 – 0.75	8.87	0.08	0.94	1.21
		0.75 – 1.00	15.8	0.1	1.9	1.05
	10 – 20	0.12 – 0.35	0.76	0.02	0.14	0.92
		0.35 – 0.55	1.51	0.02	0.21	0.88
		0.55 – 0.75	2.09	0.03	0.27	1.03
		0.75 – 1.00	6.22	0.06	0.57	1.02
	20 – 60	0.12 – 0.35	0.0048	0.0007	0.0016	1.05
		0.35 – 0.55	0.0182	0.0013	0.0031	0.84
		0.55 – 0.75	0.0403	0.0019	0.0079	0.96
		0.75 – 1.00	0.155	0.005	0.028	0.98
25 – 80	5 – 10	0.12 – 0.35	0.93	0.02	0.16	0.86
		0.35 – 0.55	1.30	0.02	0.13	0.89
		0.55 – 0.75	1.65	0.02	0.27	1.26
		0.75 – 1.00	3.97	0.03	0.46	1.06
	10 – 20	0.12 – 0.35	0.165	0.006	0.027	0.89
		0.35 – 0.55	0.330	0.007	0.045	0.91
		0.55 – 0.75	0.451	0.006	0.057	1.06
		0.75 – 1.00	1.75	0.02	0.17	1.02
	20 – 60	0.12 – 0.35	0.00246	0.00081	0.00060	1.06
		0.35 – 0.55	0.0052	0.0005	0.0015	0.88
		0.55 – 0.75	0.0071	0.0004	0.0020	0.95
		0.75 – 1.00	0.0534	0.0015	0.0097	0.98

Table 3. Triple differential dijet cross section, $\mathrm{d}^3\sigma_{2\mathrm{jet}}/\mathrm{d}Q^2\mathrm{d}y\mathrm{d}\eta^*$. See the caption of Table 2 for further details

Q^2 (GeV^2)	y	η^*	$\mathrm{d}^3\sigma_{2\mathrm{jet}}/\mathrm{d}Q^2\mathrm{d}y\mathrm{d}\eta^*$ (pb/GeV^2)	δ_{stat} (pb/GeV^2)	δ_{syst} (pb/GeV^2)	hadr. corr.
2.0 – 4.4	0.10 – 0.25	−2.5 – (−2.0)	870	10	110	0.89
		−2.0 – (−1.5)	800	10	110	1.01
		−1.5 – (−1.0)	643	11	98	1.03
		−1.0 – (−0.5)	480	8	66	0.99
		−0.5 – 0.0	404	8	64	0.94
	0.25 – 0.50	−2.5 – (−2.0)	531	7	48	1.07
		−2.0 – (−1.5)	362	5	38	1.04
		−1.5 – (−1.0)	297	5	42	0.97
		−1.0 – (−0.5)	234	4	37	0.94
		−0.5 – 0.0	193	4	30	0.92
	0.50 – 0.85	−2.5 – (−2.0)	224	4	21	1.03
		−2.0 – (−1.5)	168	3	17	0.95
		−1.5 – (−1.0)	130	2	15	0.91
		−1.0 – (−0.5)	123	3	23	0.91
		−0.5 – 0.0	109	3	18	0.88
4.4 – 10	0.10 – 0.25	−2.5 – (−2.0)	377	4	44	0.90
		−2.0 – (−1.5)	363	4	41	1.02
		−1.5 – (−1.0)	266	3	30	1.04
		−1.0 – (−0.5)	192	2	24	0.99
		−0.5 – 0.0	154	2	23	0.96
	0.25 – 0.50	−2.5 – (−2.0)	209	2	18	1.10
		−2.0 – (−1.5)	137	2	13	1.06
		−1.5 – (−1.0)	97	1	11	1.00
		−1.0 – (−0.5)	75	1	10	0.96
		−0.5 – 0.0	62.2	1.0	9.7	0.93
	0.50 – 0.85	−2.5 – (−2.0)	80.7	1.5	6.8	1.05
		−2.0 – (−1.5)	55.3	1.1	5.6	0.98
		−1.5 – (−1.0)	41.4	0.9	4.2	0.94
		−1.0 – (−0.5)	37.6	0.8	5.6	0.90
		−0.5 – 0.0	31.9	0.8	6.1	0.89
10 – 25	0.10 – 0.25	−2.5 – (−2.0)	133	1	16	0.89
		−2.0 – (−1.5)	132	1	14	1.04
		−1.5 – (−1.0)	94	1	11	1.05
		−1.0 – (−0.5)	63.7	0.8	8.0	1.04
		−0.5 – 0.0	48.3	0.7	7.9	0.97
	0.25 – 0.50	−2.5 – (−2.0)	71.2	0.8	6.3	1.11
		−2.0 – (−1.5)	45.8	0.6	4.3	1.09
		−1.5 – (−1.0)	30.8	0.4	3.0	1.01
		−1.0 – (−0.5)	23.1	0.3	2.7	0.97
		−0.5 – 0.0	17.6	0.3	2.3	0.95
	0.50 – 0.85	−2.5 – (−2.0)	25.0	0.5	2.0	1.06
		−2.0 – (−1.5)	16.4	0.3	1.5	0.99
		−1.5 – (−1.0)	12.1	0.3	1.4	0.94
		−1.0 – (−0.5)	8.4	0.2	1.3	0.93
		−0.5 – 0.0	7.3	0.2	1.2	0.91
25 – 80	0.10 – 0.25	−2.5 – (−2.0)	28.0	0.3	4.1	0.90
		−2.0 – (−1.5)	29.5	0.3	3.2	1.04
		−1.5 – (−1.0)	19.8	0.2	2.6	1.08
		−1.0 – (−0.5)	13.8	0.2	2.3	1.05
		−0.5 – 0.0	9.4	0.2	1.9	0.99
	0.25 – 0.50	−2.5 – (−2.0)	16.8	0.2	1.5	1.13
		−2.0 – (−1.5)	11.1	0.2	1.0	1.11
		−1.5 – (−1.0)	7.31	0.11	0.70	1.03
		−1.0 – (−0.5)	4.69	0.08	0.51	1.02
		−0.5 – 0.0	3.68	0.08	0.43	0.98
	0.50 – 0.85	−2.5 – (−2.0)	6.43	0.17	0.52	1.09
		−2.0 – (−1.5)	4.32	0.14	0.39	1.00
		−1.5 – (−1.0)	2.78	0.10	0.28	0.98
		−1.0 – (−0.5)	1.95	0.08	0.26	0.96
		−0.5 – 0.0	1.42	0.06	0.18	0.94

Table 4. Triple differential dijet cross section, $\mathrm{d}^3\sigma_{2\mathrm{jet}}/\mathrm{d}Q^2\mathrm{d}\eta^*\,\mathrm{d}E_T^*$. See the caption of Table 2 for further details

Q^2 (GeV^2)	η^*	E_T^* (GeV)	$\mathrm{d}^3\sigma_{2\mathrm{jet}}/\mathrm{d}Q^2\mathrm{d}\eta^*\,\mathrm{d}E_T^*$ ($\mathrm{pb/GeV}^3$)	δ_{stat} ($\mathrm{pb/GeV}^3$)	δ_{syst} ($\mathrm{pb/GeV}^3$)	hadr. corr.
2.0 – 4.4	−2.5 – (−1.7)	5 – 7	28.6	0.4	2.5	1.04
		7 – 10	54.9	0.5	5.5	0.99
		10 – 15	16.6	0.2	1.8	0.97
		15 – 20	2.78	0.05	0.42	0.94
		20 – 30	0.276	0.010	0.076	0.92
	−1.7 – (−1.3)	5 – 7	22.5	0.4	2.8	0.99
		7 – 10	35.5	0.4	4.4	1.00
		10 – 15	12.9	0.2	1.5	1.03
		15 – 20	3.50	0.08	0.47	1.00
		20 – 30	0.63	0.02	0.10	0.98
	−1.3 – 0	5 – 7	19.4	0.3	2.7	0.89
		7 – 10	24.6	0.3	3.8	0.95
		10 – 15	8.1	0.1	1.0	1.00
		15 – 20	2.07	0.04	0.29	1.00
		20 – 30	0.450	0.014	0.072	0.99
4.4 – 10	−2.5 – (−1.7)	5 – 7	11.2	0.1	1.1	1.06
		7 – 10	22.0	0.2	1.9	1.01
		10 – 15	6.85	0.06	0.84	0.99
		15 – 20	1.20	0.02	0.21	0.96
		20 – 30	0.136	0.005	0.033	0.91
	−1.7 – (−1.3)	5 – 7	7.60	0.10	0.79	1.00
		7 – 10	13.0	0.1	1.5	1.04
		10 – 15	5.22	0.06	0.50	1.03
		15 – 20	1.59	0.03	0.21	1.01
		20 – 30	0.298	0.011	0.052	0.97
	−1.3 – 0	5 – 7	6.16	0.06	0.68	0.91
		7 – 10	8.3	0.1	1.1	0.97
		10 – 15	3.02	0.03	0.35	1.00
		15 – 20	0.88	0.01	0.12	1.01
		20 – 30	0.199	0.005	0.031	1.00
10 – 25	−2.5 – (−1.7)	5 – 7	3.64	0.04	0.32	1.06
		7 – 10	7.41	0.05	0.64	1.02
		10 – 15	2.41	0.02	0.29	0.99
		15 – 20	0.445	0.007	0.071	0.94
		20 – 30	0.045	0.002	0.011	0.93
	−1.7 – (−1.3)	5 – 7	2.39	0.03	0.25	1.03
		7 – 10	4.27	0.04	0.46	1.06
		10 – 15	1.86	0.02	0.17	1.05
		15 – 20	0.529	0.010	0.075	1.01
		20 – 30	0.098	0.003	0.017	0.96
	−1.3 – 0	5 – 7	1.80	0.02	0.20	0.94
		7 – 10	2.41	0.02	0.30	0.98
		10 – 15	0.98	0.01	0.11	1.03
		15 – 20	0.313	0.005	0.040	1.02
		20 – 30	0.078	0.002	0.011	1.00
25 – 80	−2.5 – (−1.7)	5 – 7	0.741	0.009	0.087	1.12
		7 – 10	1.58	0.01	0.17	1.04
		10 – 15	0.589	0.006	0.072	0.99
		15 – 20	0.134	0.002	0.024	0.94
		20 – 30	0.0143	0.0006	0.0046	0.92
	−1.7 – (−1.3)	5 – 7	0.451	0.007	0.057	1.00
		7 – 10	0.91	0.01	0.10	1.09
		10 – 15	0.471	0.006	0.050	1.05
		15 – 20	0.163	0.003	0.023	1.00
		20 – 30	0.0324	0.0012	0.0068	0.99
	−1.3 – 0	5 – 7	0.301	0.004	0.041	0.98
		7 – 10	0.477	0.005	0.064	1.03
		10 – 15	0.238	0.003	0.030	1.05
		15 – 20	0.090	0.002	0.010	1.02
		20 – 30	0.0229	0.0007	0.0042	1.00

Table 5. Triple differential event cross section, $\mathrm{d}^3\sigma_{\mathrm{ep}}/\mathrm{d}Q^2\mathrm{d}x_\gamma^{\mathrm{jets}}\mathrm{d}y$. See the caption of Table 2 for further details

Q^2 (GeV^2)	x_γ	y	$\mathrm{d}^3\sigma_{\mathrm{ep}}/\mathrm{d}Q^2\mathrm{d}x_\gamma^{\mathrm{jets}}\mathrm{d}y$ (pb/GeV^2)	δ_{stat} (pb/GeV^2)	δ_{syst} (pb/GeV^2)	hadr. corr.
2.0 – 4.4	0 – 0.75	0.10 – 0.25	586	12	100	0.98
		0.25 – 0.40	409	9	63	0.93
		0.40 – 0.55	283	7	41	0.88
		0.55 – 0.70	199	5	27	0.86
		0.70 – 0.85	192	8	27	0.87
	0.75 – 1	0.10 – 0.25	1360	31	200	0.96
		0.25 – 0.40	653	15	63	1.11
		0.40 – 0.55	289	9	25	1.15
		0.55 – 0.70	164	7	14	1.13
		0.70 – 0.85	89.6	6.2	7.3	1.12
4.4 – 10	0 – 0.75	0.10 – 0.25	198	3	27	0.99
		0.25 – 0.40	126	2	17	0.95
		0.40 – 0.55	92	2	12	0.90
		0.55 – 0.70	66.9	2.1	9.1	0.88
		0.70 – 0.85	53.6	2.2	7.1	0.88
	0.75 – 1	0.10 – 0.25	744	11	74	0.97
		0.25 – 0.40	291	6	30	1.12
		0.40 – 0.55	138	4	12	1.17
		0.55 – 0.70	69.0	2.8	5.5	1.15
		0.70 – 0.85	34.3	2.4	2.7	1.15
10 – 25	0 – 0.75	0.10 – 0.25	58.8	0.9	8.6	1.04
		0.25 – 0.40	37.8	0.7	4.6	0.97
		0.40 – 0.55	25.0	0.6	3.1	0.91
		0.55 – 0.70	17.5	0.5	2.2	0.91
		0.70 – 0.85	13.4	0.7	1.5	0.88
	0.75 – 1	0.10 – 0.25	294	4	30	0.97
		0.25 – 0.40	112	2	12	1.13
		0.40 – 0.55	49.6	1.4	4.0	1.17
		0.55 – 0.70	24.0	1.0	1.8	1.14
		0.70 – 0.85	12.35	0.84	0.91	1.14
25 – 80	0 – 0.75	0.10 – 0.25	9.5	0.2	1.8	1.07
		0.25 – 0.40	6.98	0.15	0.85	1.04
		0.40 – 0.55	5.00	0.15	0.51	0.97
		0.55 – 0.70	3.32	0.17	0.36	0.93
		0.70 – 0.85	2.25	0.27	0.22	0.92
	0.75 – 1	0.10 – 0.25	72.5	0.9	8.6	0.98
		0.25 – 0.40	31.4	0.6	2.9	1.12
		0.40 – 0.55	15.0	0.5	1.3	1.14
		0.55 – 0.70	8.99	0.47	0.88	1.16
		0.70 – 0.85	4.01	0.57	0.85	1.13

NLO. The description of the data for $x_\gamma^{\mathrm{jets}} < 0.75$ gets worse as Q^2 and E_T^* decrease. The discrepancy is particularly pronounced at small x_γ^{jets}, low Q^2 and low E_T^*, where the data lie significantly above the theoretical predictions, even taking into account the sizable scale uncertainty. The relative decrease of the cross section at low x_γ^{jets} as E_T^* increases is of kinematic origin, due to the restrictions in the available phase space. Note that for $x_\gamma^{\mathrm{jets}} < 0.75$, the JETVIP results are systematically lower than those of DISENT, whereas for $x_\gamma^{\mathrm{jets}} > 0.75$ the opposite effect is observed. The discrepancy between DISENT and JETVIP is observed only for multi-differential distributions which

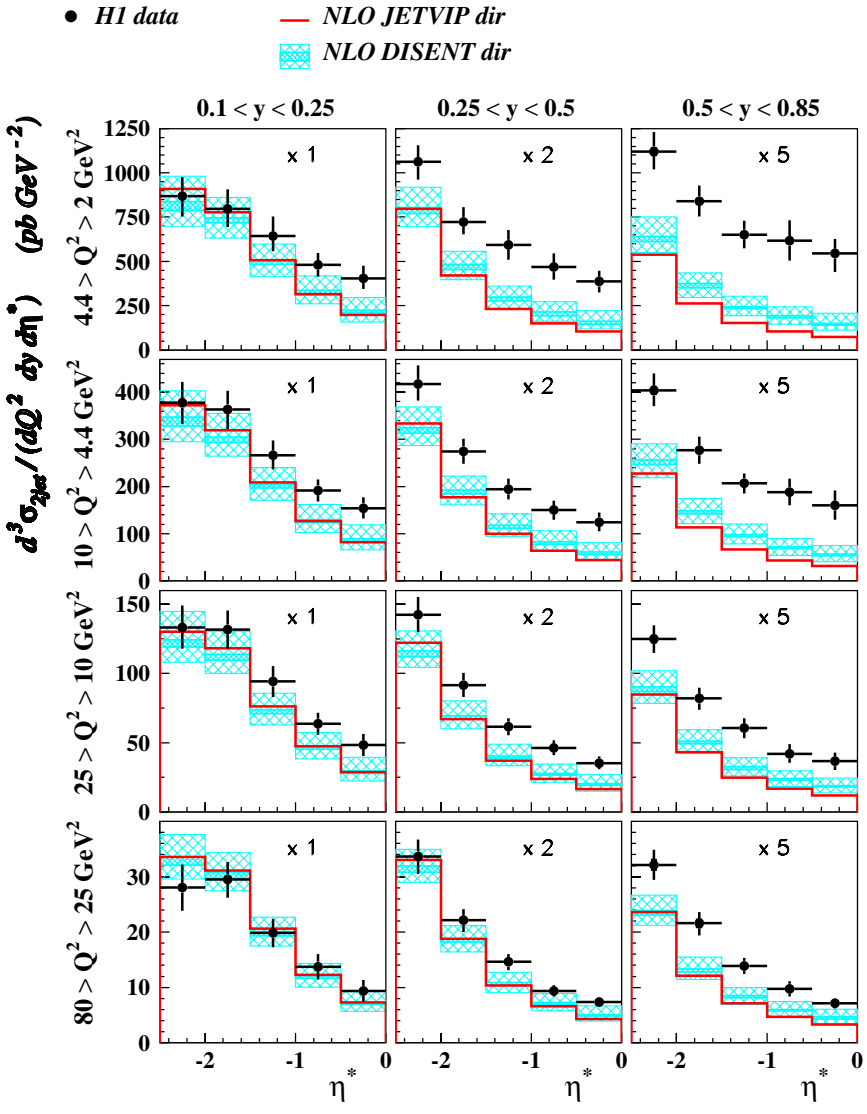

Fig. 3. Triple differential dijet cross section, $\mathrm{d}^3\sigma_{2\mathrm{jet}}/\mathrm{d}Q^2\mathrm{d}y\mathrm{d}\eta^*$. Negative values of η^* correspond to the photon fragmentation region. See the caption of Fig. 2 for further details

include a jet variable.[8] It gets substantially smaller for the inclusive dijet cross section $\mathrm{d}^2\sigma_{\mathrm{ep}}/\mathrm{d}Q^2\mathrm{d}y$ [22] (not shown) and agrees within 2% for the total dijet cross section in our kinematic region. A similar level of agreement between JETVIP and DISENT was reported in [54] for the total dijet cross section.

The data were also analysed in terms of jet pseudorapidities. Figure 3 presents the dijet cross section as a function of η^* in different bins of Q^2 and y, where η^* denotes the pseudorapidities of the jets with the highest and second highest E_T^* in the photon-proton centre-of-mass system, such that each event enters the distributions twice. The excess of the data over the theory at low Q^2 and low x_γ^{jets} observed in Fig. 2 is reflected in Fig. 3 in a similar excess at low Q^2 and high y, which is especially pronounced in the forward region of the laboratory frame ($\eta^* \sim 0$).

[8] The results obtained with DISENT have been cross checked with NLO dijet calculations using NLOJET [53], which is also based on the subtraction method.

Figure 4 shows the triple differential dijet cross section as a function of E_T^* in different bins of Q^2 and η^*, each event entering the distributions twice. The predictions of the NLO direct calculations agree well with the data at large Q^2 or at large E_T^* for all η^*. On the other hand, the predictions clearly fail to describe the data in the forward region at low Q^2 and low E_T^*. The low E_T^* region is better described as η^* is reduced or Q^2 is increased. A similar discrepancy between the data and the NLO prediction has recently been reported for inclusive jet cross sections in a similar kinematic region [4]. The measurement in [4] indicated that the region where the NLO calculations fail to describe the data corresponds to the region where the ratio of NLO to LO predictions is largest. The same is true for the dijet cross sections. The NLO corrections are smallest in the backward region at the largest Q^2 and E_T^*, where the ratio is approximately 1.1. The data are well described by the NLO direct calculations in this kinematic region, as can be seen in Fig. 4. On the other hand, the ratio of NLO to LO predictions for the forward region at small Q^2

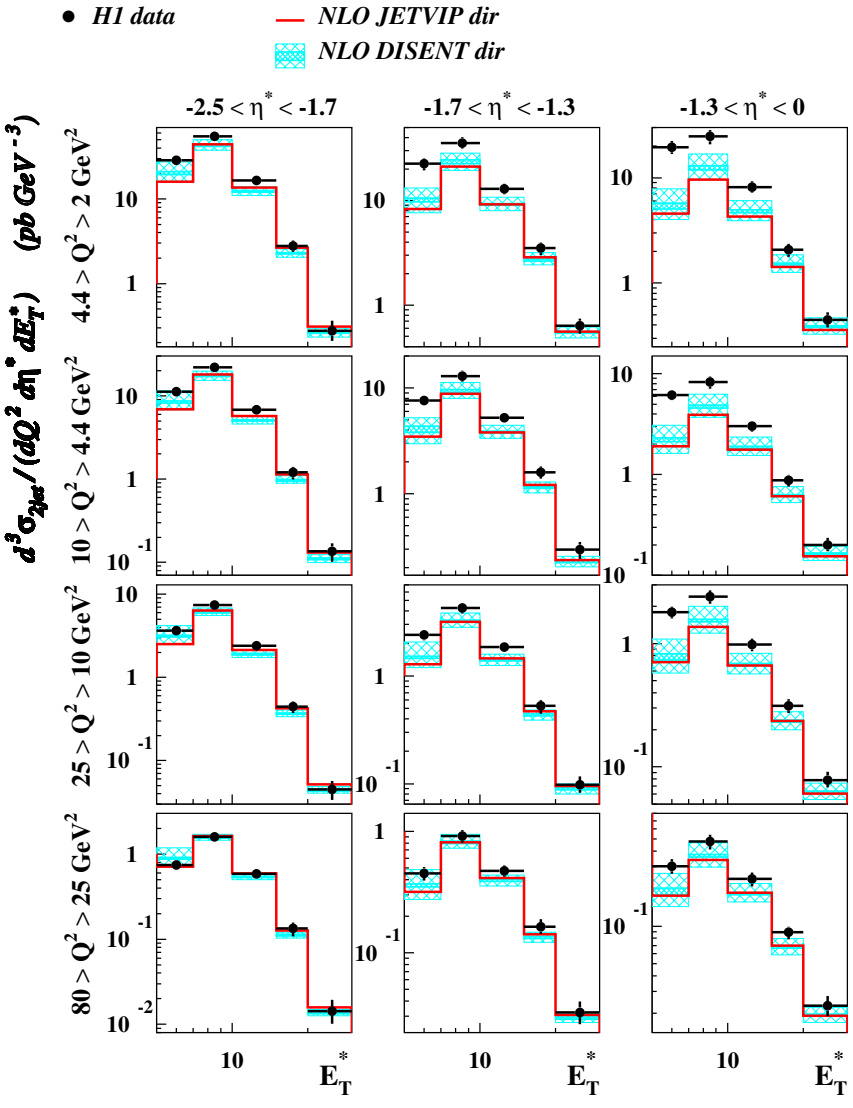

Fig. 4. Triple differential dijet cross section, $\mathrm{d}^3\sigma_{2\mathrm{jet}}/\mathrm{d}Q^2\mathrm{d}\eta^*\,\mathrm{d}E_T^*$. Negative values of η^* correspond to the photon fragmentation region. See the caption of Fig. 2 for further details

and E_T^* becomes as large as 9 and the data there are not reproduced by the NLO calculations. Corrections beyond NLO are therefore expected to improve the description in this region.

The above comparisons show that in the region of low Q^2, high y, forward η^* and low E_T^* the data lie significantly above NLO QCD calculations for direct photons. This excess cannot be accommodated within standard theoretical uncertainties from scale variations and hadronisation corrections.

6.2 Resolved virtual photons

The pattern of the observed discrepancy between the data and the NLO calculations in Fig. 2–4 suggests an explanation in terms of the interactions of resolved virtual photons, understood as an approximation to contributions beyond NLO. Of the NLO parton level calculations, only JETVIP includes a resolved virtual photon contribution[9]. Unfortunately, the dependence on the slicing parameter y_c of the NLO JETVIP calculations of the resolved γ_T^* contribution (i.e. up to order $\alpha\alpha_s^3$) is much larger than for the direct component [22], and the resulting calculations are therefore less reliable. In the absence of other calculations of this kind, the data are compared with the results of the full JETVIP calculations in Fig. 2 using $y_c = 0.003$ (see Sect. 2.3), in order to see the qualitative effects of resolved photon interactions at NLO.

The inclusion of a resolved γ_T^* contribution brings the NLO calculations closer to the data, though there is still a discrepancy between the data and calculations at low to moderate x_γ^{jets} and low Q^2. The dominant part of the difference between the full NLO JETVIP results and the direct component comes from the $\mathcal{O}(\alpha\alpha_s^3)$ term in the resolved γ_T^* contribution (Fig. 1e). Including only the lead-

[9] Only the contribution of transversely polarised resolved photons is implemented in JETVIP.

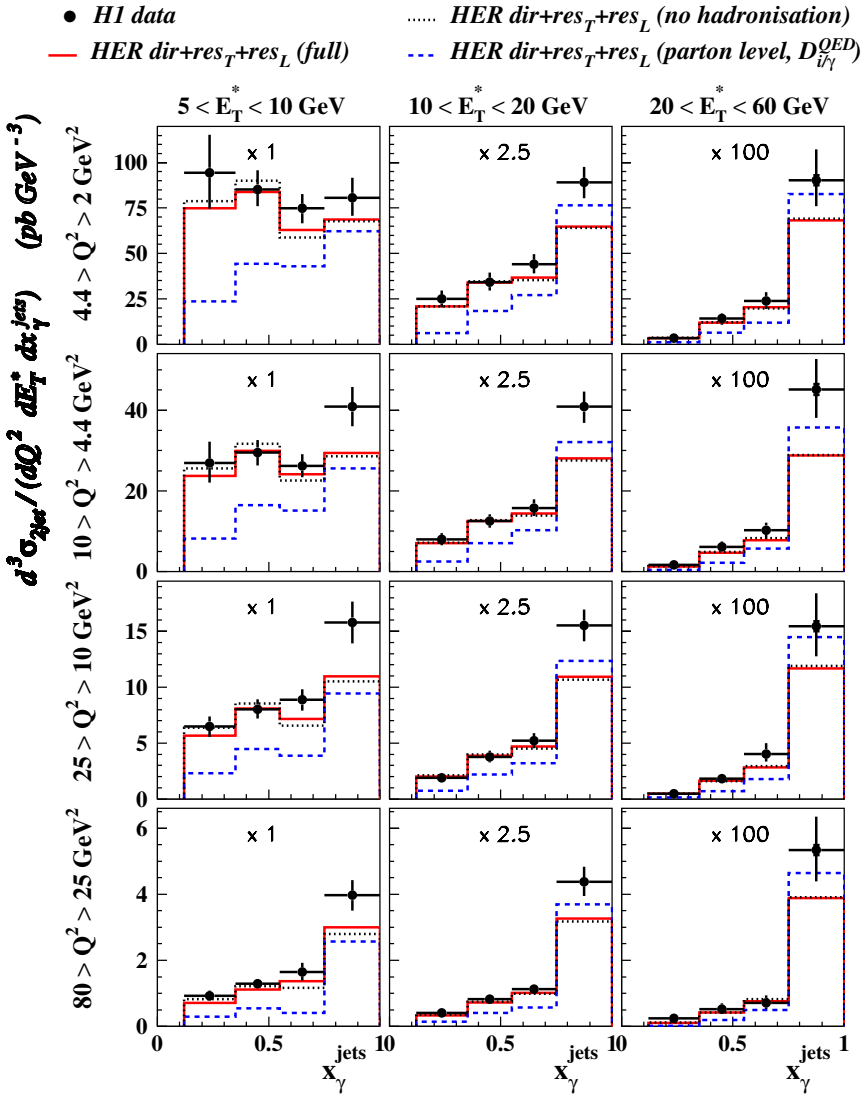

Fig. 5. The triple differential dijet cross section, $\mathrm{d}^3\sigma_{2\mathrm{jet}}/\mathrm{d}Q^2\mathrm{d}E_T^*\,\mathrm{d}x_\gamma^{\mathrm{jets}}$, from H1 data, compared with the predictions of the full HERWIG simulation as defined in Sect. 2.3 (full line), HERWIG without hadronisation or soft underlying event effects (dotted line) and HERWIG at the parton level without parton showers (dashed line). In the latter case, the QED PDFs of γ_T^* and γ_L^* [see (5) and (7)] are used in the resolved photon contributions

ing resolved γ_T^* terms (Fig. 1c,d) has only a small effect [22].

6.3 Comparison with DGLAP Monte Carlo models

In this section, the data are compared with the predictions of the HERWIG Monte Carlo event generator, which combines proton PDFs obtained from global LO QCD fits [36] with LO parton level cross sections. Unlike the NLO parton level calculations, DISENT and JETVIP, discussed in the context of Fig. 2–4, LO MC models take initial and final state QCD parton showers into account. Although theoretical uncertainties are difficult to quantify, MC models can be used to estimate the influence of modifications to the theoretical modelling such as the effects of parton showers, the QCD improvements of D_{i/γ^*} (see (2)) and the simulation of soft underlying interactions and hadronisation. The relative importance of these effects is investigated in Fig. 5. The full HERWIG simulation, as described in Sect. 2.3, is compared with the HERWIG prediction without hadronisation or soft underlying event effects, and with the HERWIG calculation at the parton level without parton showers and with only the QED PDFs of virtual photons. The cross sections predicted by the full HERWIG simulation are in good agreement with the data in the low x_γ^{jets} region. The highest x_γ^{jets} region is not described so well. The largest difference between the cross section predicted by the full HERWIG simulation and that obtained from the parton level calculation comes from the initial and final state QCD parton showers, which effectively introduce an intrinsic k_T of the partons in the incoming proton. These effects increase the total dijet cross section in our kinematic region typically by 30% and by as much as 100% at low Q^2, low E_T^* and low x_γ^{jets}. Another 10% increase of the total dijet cross section arises from the change from QED to QCD-improved D_{i/γ^*}. Soft underlying events increase the total dijet cross section by 4%. Their influence is largest in the region of low Q^2, low E_T^* and low x_γ^{jets}, where the cross section is increased by 10%. A similar effect is observed when using the multiple interaction model implemented in PYTHIA.

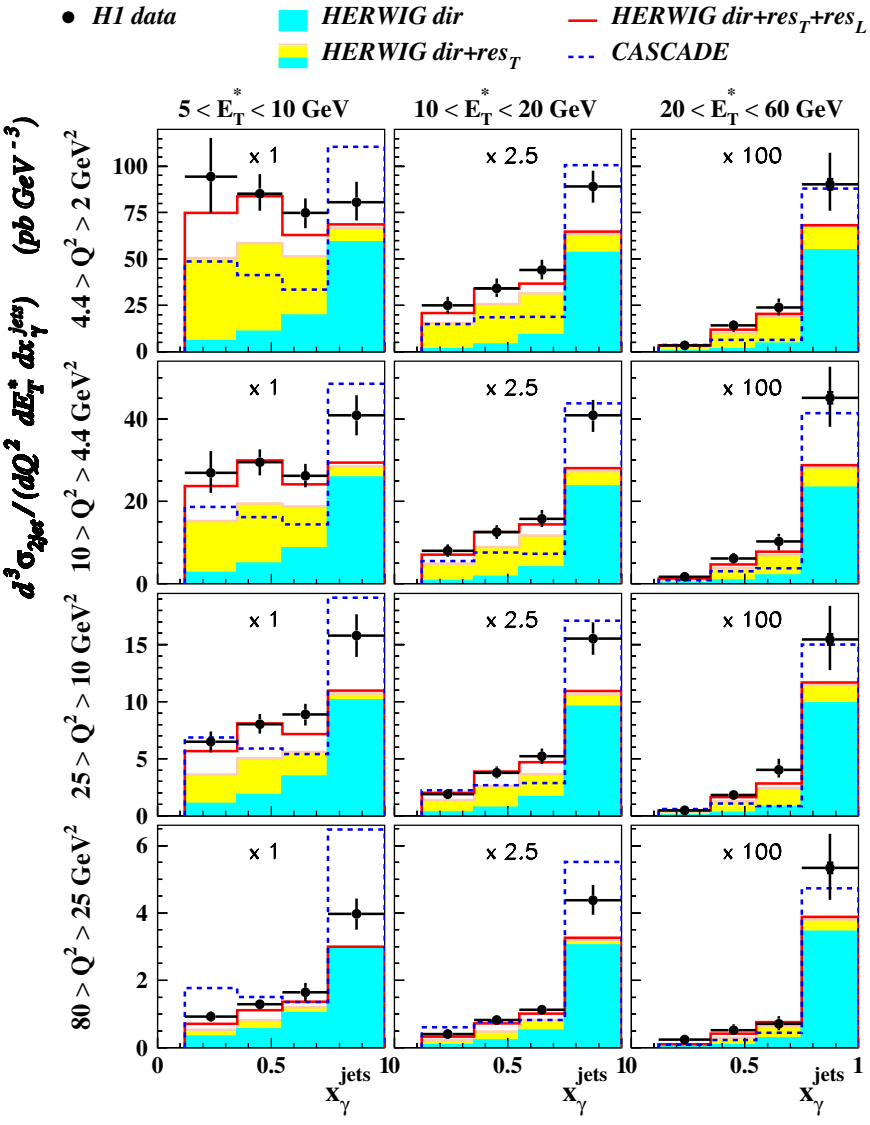

Fig. 6. The triple differential dijet cross section, $\mathrm{d}^3\sigma_{2\mathrm{jet}}/\mathrm{d}Q^2\mathrm{d}E_T^*\,\mathrm{d}x_\gamma^{\mathrm{jets}}$, from H1 data compared with the predictions of HERWIG and CASCADE. The dark-filled histograms show the direct HERWIG contribution. The light-filled histograms the resolved γ_T^* HERWIG prediction and the full line is the sum of all direct, γ_T^* and γ_L^* resolved HERWIG contributions

Previous analyses of jet production in low Q^2 ep collisions have compared with resolved virtual photon models that neglect longitudinally polarised photons. Figure 6 shows predictions of the direct and γ_T^* and γ_L^* resolved photon components separately. At high Q^2 the HERWIG direct photon prediction alone reasonably describes the shape of the x_γ^{jets} distribution of the data, while at low Q^2 the resolved photon contributions are clearly needed. The contribution of longitudinally polarised resolved photons improves the agreement with the data. Not only do they increase the magnitude of the HERWIG predictions such that they become closer to data, but they also correctly reproduce the Q^2 and E_T^* dependence. For a given interval of E_T^* , the ratio of γ_L^* to γ_T^* contributions increases with Q^2, whereas keeping Q^2 fixed it decreases with increasing E_T^* . This behaviour is expected from (5) and (6). Enhancing the PDF of γ_T^* in the resolved photon contribution by a constant factor does not lead to a comparably successful description of the data.

As a result of the different y dependences of the photon fluxes in (3) and (4), the dijet cross section as a function of y is different for longitudinal and transverse photons. Figure 7 shows the event cross section as a function of y in different bins of Q^2 and x_γ^{jets}. In contrast to all previous dijet cross sections, each event contributes only once to the event cross section $\mathrm{d}^3\sigma_{\mathrm{ep}}/\mathrm{d}Q^2\mathrm{d}x_\gamma^{\mathrm{jets}}\mathrm{d}y$. The ratio of longitudinally to transversely polarised photons decreases with increasing y, as expected from the fluxes (see (3) and (4)). The addition of the resolved longitudinal photon contribution brings the HERWIG predictions[10] closer to the data. The small contribution of γ_L^* compared to γ_T^* at

[10] The low HERWIG prediction for all bins with $x_\gamma^{\mathrm{jets}} > 0.75$ and at the lowest y for $x_\gamma^{\mathrm{jets}} < 0.75$ is partially due to a cut-off procedure in HERWIG, which suppresses the PDF of the virtual photon at large x_γ^{jets}. The resolved γ_T^* contribution of RAPGAP (not shown) leads to a rise with decreasing y that is similar to that in the data for the low x_γ^{jets} range, though RAPGAP also lies below the data in the large x_γ^{jets} range [22].

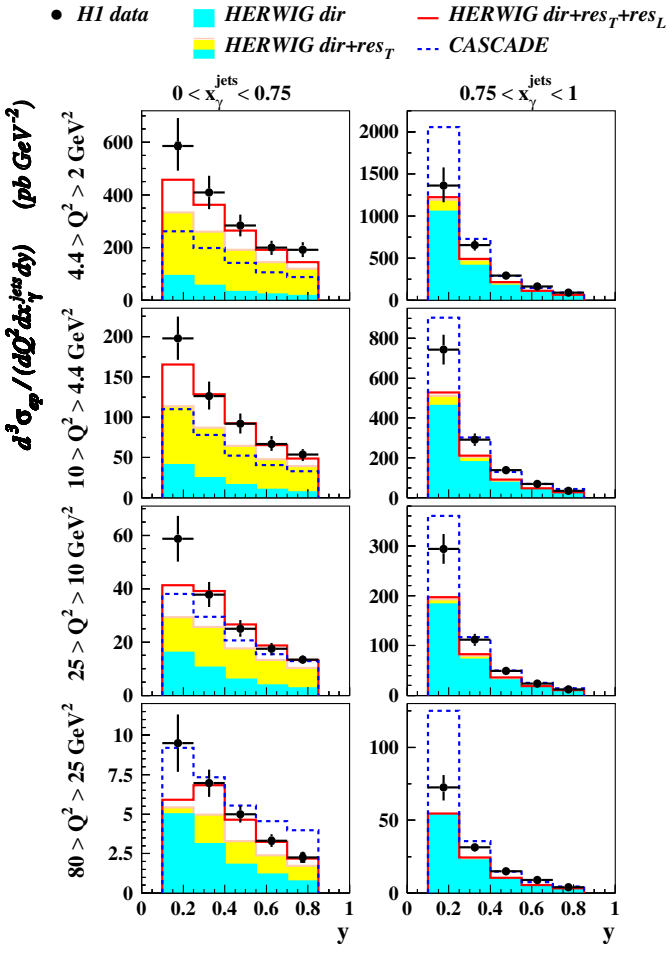

Fig. 7. Triple differential event cross section, $\mathrm{d}^3\sigma_{\mathrm{ep}}/\mathrm{d}Q^2\mathrm{d}x_\gamma^{\mathrm{jets}}\mathrm{d}y$. See the caption of Fig. 6 for further details

large x_γ^{jets} is a consequence of the different x_γ dependences of D_{i/γ_T^*} and D_{i/γ_L^*} (see (5) and (6)).

Figure 8 compares the measured dijet cross section as a function of η^* in different bins of Q^2 and y, presented already in Fig. 3, with the HERWIG prediction. The data are well reproduced by the complete LO MC model in shape. However, the absolute normalisation is not satisfactory, especially at low y. In agreement with the conclusion of Figs. 6 and 7, the importance of the resolved photon contributions increases in the forward jet region ($\eta^* \sim 0$), for low Q^2 and at high y.

6.4 Comparison with CCFM Monte Carlo model

In Figs. 6-8, the data are also compared with the predictions of the CASCADE MC, employing the unintegrated PDF (set 1 of [37]) with the CCFM evolution equations.

The CASCADE prediction describes the main qualitative trends in the data, except the Q^2 dependence in the lowest E_T^* bin (Fig. 6) or at low x_γ^{jets} (Fig. 7). CASCADE also overestimates the data in the lowest y bin at high x_γ^{jets} (Fig. 7). On the other hand, CASCADE predicts a significant dijet cross section at low x_γ^{jets} (Fig. 6), much higher and closer to the data than the LO and NLO DGLAP predictions without the resolved photon interactions. Also, except for the highest Q^2 bin, dijet production in the forward region is reproduced better by CASCADE (Fig. 8) than by NLO direct photon calculations (Fig. 3).

Large sensitivity of the CASCADE predictions to the choice of unintegrated proton PDF is observed [22]. The results shown here are based on set 1 of [37], where only the singular terms in the gluon splitting function are included. Switching to set 2 of [37], for which the full gluon splitting function is used, results in a reduction in the predicted cross section by a small factor at large x_γ^{jets}, increasing up to around 30 % at low x_γ^{jets}. Set 2 gives the best description for different observables in another recent dijet measurement covering a similar kinematic region [3].

7 Summary

Triple differential dijet cross sections in $e^{\pm}p$ interactions are measured in the region of photon virtualities $2 < Q^2 < 80\,\mathrm{GeV}^2$ and over a wide range of inelasticities $0.1 < y < 0.85$. The data, covering the kinematic range $E_{T\,1}^* > 7\,\mathrm{GeV}$, $E_{T\,2}^* > 5\,\mathrm{GeV}$ and pseudorapidities $-2.5 < \eta_1^*, \eta_2^* < 0$, are compared with NLO and LO calculations, with and without resolved photon contributions or parton showers, as well as with a calculation based on k_T factorisation and an unintegrated PDF of the proton.

A sizable and systematic excess of the data over NLO calculations which do not include a resolved virtual photon contribution, is observed for $Q^2 < 10\,\mathrm{GeV}^2$, small jet transverse energies, E_T^*, and small x_γ^{jets}, or equivalently, large jet pseudorapidities, η^*. The excess observed for $x_\gamma^{\mathrm{jets}} < 0.75$ decreases with increasing Q^2.

NLO QCD calculations incorporating a resolved virtual photon, as implemented in JETVIP, bring the QCD predictions closer to the data, though there is still a deficit at low x_γ^{jets}, especially for low Q^2. Unfortunately the JETVIP prediction for the resolved part of the dijet cross section is sensitive to the choice of the slicing parameter y_c and must therefore be taken with caution.

The significant role of initial and final state QCD parton showers, which are not taken into account in the NLO QCD calculations, is illustrated. The inclusion of QCD parton showers in the HERWIG LO Monte Carlo model leads to a considerable improvement in the description, though a discrepancy remains in the region of high x_γ^{jets}. Within this model, the best agreement with the data is obtained when both transversely and longitudinally polarised resolved virtual photons are included.

CASCADE, which is based on the CCFM evolution scheme, does not involve the concept of virtual photon structure. The CASCADE description of the data is best in the region of moderate Q^2 between 10 and 25 GeV^2. The Q^2 dependence of the cross section is less steep than in the data.

To conclude, the data show clear evidence for effects that go beyond the fixed-order NLO QCD calculations.

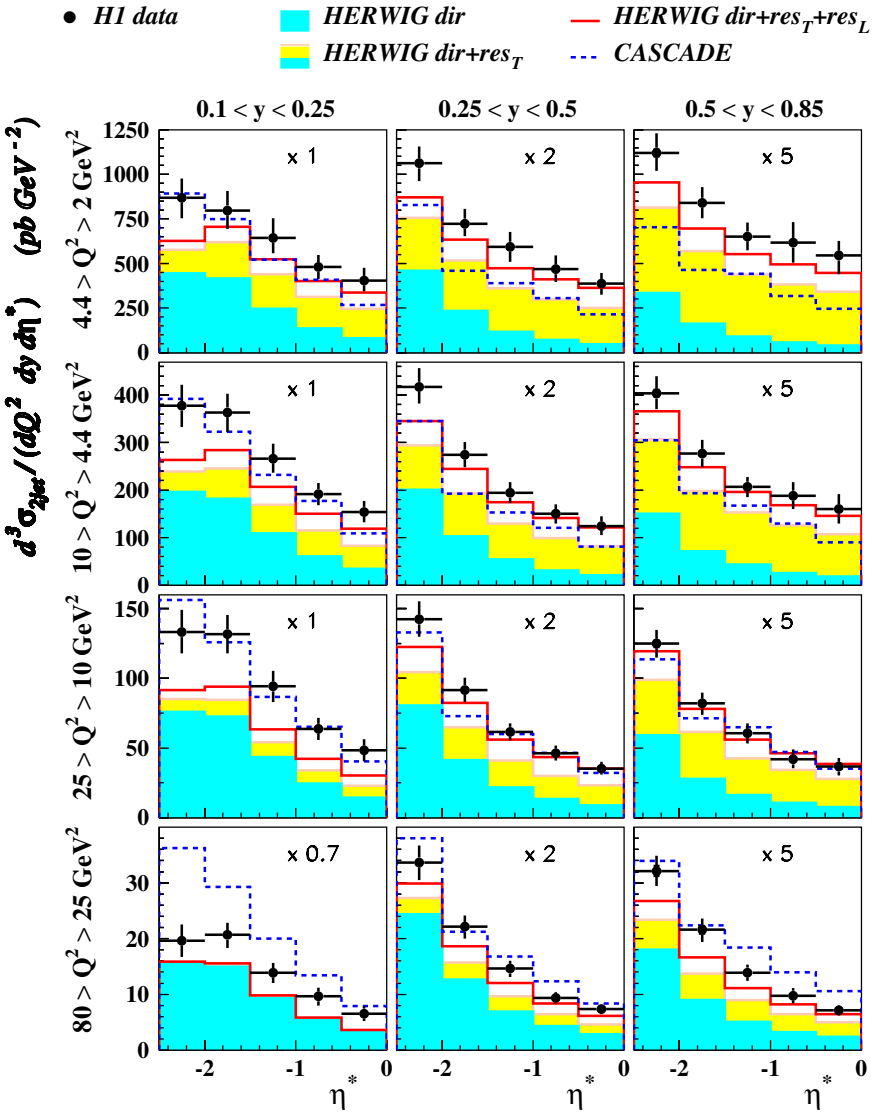

Fig. 8. Triple differential dijet cross section, $\mathrm{d}^3\sigma_{2\mathrm{jet}}/\mathrm{d}Q^2\mathrm{d}y\mathrm{d}\eta^*$. See the caption of Fig. 6 for further details

The importance of QCD parton showers and of the resolved γ_L^* contribution is illustrated within the context of the HERWIG LO Monte Carlo model.

Acknowledgements. We are grateful to the HERA machine group whose outstanding efforts have made this experiment possible. We thank the engineers and technicians for their work in constructing and maintaining the H1 detector, our funding agencies for financial support, the DESY technical staff for continual assistance and the DESY directorate for support and for the hospitality which they extend to the non-DESY members of the collaboration.

References

1. C. Adloff et al. [H1 Collaboration], Eur. Phys. J. C **19**, 429 (2001) [hep-ex/0010016]; C. Adloff et al. [H1 Collaboration], Phys. Lett. B **515**, 17 (2001) [hep-ex/0106078]; C. Adloff *et al.* [H1 Collaboration], Eur. Phys. J. C **25**, 13 (2002) [hep-ex/0201006]; C. Adloff et al. [H1 Collaboration], Eur. Phys. J. C **29**, 497 (2003) [hep-ex/0302034]
2. S. Chekanov et al. [ZEUS Collaboration], Eur. Phys. J. C **23**, 13 (2002) [hep-ex/0109029]; S. Chekanov et al. [ZEUS Collaboration], Phys. Lett. B **547**, 164 (2002) [hep-ex/0208037]; S. Chekanov et al. [ZEUS Collaboration], Phys. Lett. B **551**, 226 (2003) [hep-ex/0210064]; S. Chekanov et al. [ZEUS Collaboration], Phys. Lett. B **560**, 7 (2003) [hep-ex/0212064]
3. A. Aktas et al. [H1 Collaboration], DESY 03-160, submitted to Eur. Phys. J. C [hep-ex/0310019]
4. C. Adloff et al. [H1 Collaboration], Phys. Lett. B **542**, 193 (2002) [hep-ex/0206029]
5. S. Chekanov et al. [ZEUS Collaboration], Eur. Phys. J. C **23**, 615 (2002) [hep-ex/0112029]
6. C. Adloff et al. [H1 Collaboration], Eur. Phys. J. C **19**, 289 (2001) [hep-ex/0010054]
7. J. Breitweg et al. [ZEUS Collaboration], Phys. Lett. B **479**, 37 (2000) [hep-ex/0002010]
8. J. Breitweg et al. [ZEUS Collaboration], Eur. Phys. J. C **11**, 35 (1999) [hep-ex/9905046]

9. S. Chekanov et al. [ZEUS Collaboration], Eur. Phys. J. C **35**, 487 (2004) [hep-ex/0404033]
10. R. Nisius, Phys. Rept. **332**, 165 (2000) [hep-ex/9912049]
11. M. Krawczyk, A. Zembrzuski, M. Staszel, Phys. Rept. **345**, 265 (2001) [hep-ph/0011083]; K. Sasaki, J. Soffer, T. Uematsu, Phys. Rev. D **66**, 034014 (2002) [hep-ph/0205159]
12. G.A. Schuler, T. Sjöstrand, Phys. Lett. B **376**, 193 (1996) [hep-ph/9601282]
13. M. Glück, E. Reya, M. Stratmann, Phys. Rev. D **54**, 5515 (1996) [hep-ph/9605297]; M. Glück, E. Reya, I. Schienbein, Phys. Rev. D **60**, 054019 (1999) [Erratum-ibid. D **62**, 019902 (2000)] [hep-ph/9903337]
14. G. Kramer, B. Pötter, Eur. Phys. J. C **5**, 665 (1998) [hep-ph/9804352]
15. J. Chýla, M. Taševský, Phys. Rev. D **62**, 114025 (2000) [hep-ph/9912514]
16. C. Adloff et al. [H1 Collaboration], Eur. Phys. J. C **13**, 397 (2000) [hep-ex/9812024]
17. C. Adloff et al. [H1 Collaboration], Phys. Lett. B **415**, 418 (1997) [hep-ex/9709017]
18. V.N. Gribov, L.N. Lipatov, Yad. Fiz. **15**, 781 (1972) [Sov. J. Nucl. Phys. **15**, 438 (1972)]; V.N. Gribov, L.N. Lipatov, Yad. Fiz. **15**, 1218 (1972) [Sov. J. Nucl. Phys. **15**, 675 (1972)]; L.N. Lipatov, Sov. J. Nucl. Phys. **20**, 94 (1975) [Yad. Fiz. **20**, 181 (1974)]; G. Altarelli, G. Parisi, Nucl. Phys. B **126**, 298 (1977); Y.L. Dokshitzer, Sov. Phys. JETP **46**, 641 (1977) [Zh. Eksp. Teor. Fiz. **73** 1216 (1977)]
19. J. Chýla, Phys. Lett. B **488**, 289 (2000) [hep-ph/0006232]
20. C. Friberg, T. Sjöstrand, Phys. Lett. B **492**, 123 (2000) [hep-ph/0009003]
21. J. Chýla, M. Taševský, Eur. Phys. J. C **16**, 471 (2000) [hep-ph/0003300]; J. Chýla, M. Taševský, Eur. Phys. J. C **18**, 723 (2001) [hep-ph/0010254]
22. K. Sedlák, "Measurement of Dijet Production at Low Q^2 at HERA", Ph.D. Thesis, Institute of Physics, Academy of Sciences of the Czech Republic, Praha, available from http://www-h1.desy.de/h1/www/publications/theses_list.html
23. M. Ciafaloni, Nucl. Phys. B **296**, 49 (1988); S. Catani, F. Fiorani, G. Marchesini, Phys. Lett. B **234**, 339 (1990); S. Catani, F. Fiorani, G. Marchesini, Nucl. Phys. B **336**, 18 (1990); G. Marchesini, Nucl. Phys. B **445**, 49 (1995) [hep-ph/9412327]
24. B. Andersson et al. [Small x Collaboration], Eur. Phys. J. C **25**, 77 (2002) [hep-ph/0204115]
25. H. Jung, L. Jönsson, H. Küster, DESY-98-051, LUNFD6-NFFL-7156-1998, [hep-ph/9805396]; H. Jung, L. Jönsson, H. Küster, Proceedings of Workshop on Photon Interactions and the Photon Structure, p. 229, Lund, Sweden, 10–13 Sep 1998, [hep-ph/9811368]; H. Jung, L. Jönsson, H. Küster, Eur. Phys. J. C **9**, 383 (1999) [hep-ph/9903306]
26. G. Marchesini et al., Comput. Phys. Commun. **67**, 465 (1992)
27. H. Jung, Comput. Phys. Commun. **86**, 147 (1995)
28. T. Sjöstrand, Comput. Phys. Commun. **39**, 347 (1986); T. Sjöstrand, M. Bengtsson, Comput. Phys. Commun. **43**, 367 (1987)
29. T. Sjöstrand, Comput. Phys. Commun. **82**, 74 (1994); T. Sjöstrand, L. Lönnblad, S. Mrenna, [hep-ph/0108264]; T. Sjöstrand et al., Comput. Phys. Commun. **135**, 238 (2001) [hep-ph/0010017]
30. S. Catani, M.H. Seymour, Nucl. Phys. B **485**, 291 (1997) [Erratum-ibid. B **510**, 503 (1997)] [hep-ph/9605323]
31. R.K. Ellis, D.A. Ross, A.E. Terrano, Nucl. Phys. B **178**, 421 (1981)
32. B. Pötter, Comput. Phys. Commun. **119**, 45 (1999) [hep-ph/9806437]
33. B. Pötter, Comput. Phys. Commun. **133**, 105 (2000) [hep-ph/9911221]
34. H. Jung, G.P. Salam, Eur. Phys. J. C **19**, 351 (2001) [hep-ph/0012143]; H. Jung, Comput. Phys. Commun. **143**, 100 (2002) [hep-ph/0109102]
35. H. Jung, Phys. Rev. D **65**, 034015 (2002) [hep-ph/0110034]
36. H.L. Lai et al., Eur. Phys. J. C **12**, 375 (2000) [hep-ph/9903282]
37. M. Hansson, H. Jung, Status of CCFM: Un-integrated gluon densities, talk given at the XI Int. Workshop on Deep Inelastic Scattering (DIS 2003), St. Petersburg, Russia 2003, to appear in the proceedings [hep-ph/0309009]
38. G. Ingelman, A. Edin, J. Rathsman, Comput. Phys. Commun. **101**, 108 (1997) [hep-ph/9605286]
39. I. Abt et al. [H1 Collaboration], Nucl. Instrum. Meth. A **386**, 310 (1997); I. Abt et al. [H1 Collaboration], Nucl. Instrum. Meth. A **386**, 348 (1997)
40. J. Bürger et al., Nucl. Instrum. Meth. A **279**, 217 (1989)
41. B. Andrieu et al. [H1 Calorimeter Group], Nucl. Instrum. Meth. A **336**, 460 (1993)
42. B. Andrieu et al. [H1 Calorimeter Group], Nucl. Instrum. Meth. A **350**, 57 (1994); B. Andrieu et al. [H1 Calorimeter Group], Nucl. Instrum. Meth. A **336**, 499 (1993)
43. R.D. Appuhn et al. [H1 SPACAL Group], Nucl. Instrum. Meth. A **386**, 397 (1997)
44. T. Nicholls et al. [H1 SPACAL Group], Nucl. Instrum. Meth. A **374**, 149 (1996)
45. H1 Collaboration, "Technical Proposal for the Upgrade of the Backward Region of the H1 Detector", DESY internal report PRC-93/02
46. S.D. Ellis, D.E. Soper, Phys. Rev. D **48**, 3160 (1993) [hep-ph/9305266]; S. Catani et al., Nucl. Phys. B **406**, 187 (1993)
47. C. Adloff et al. [H1 Collaboration], Z. Phys. C **74**, 221 (1997) [hep-ex/9702003]
48. M. Klasen, G. Kramer, Phys. Lett. B **366**, 385 (1996) [hep-ph/9508337]; M. Klasen, G. Kramer, Z. Phys. C **76**, 67 (1997) [hep-ph/9611450]; S. Frixione, G. Ridolfi, Nucl. Phys. B **507**, 315 (1997) [hep-ph/9707345]
49. J. Chýla, K. Sedlák, "Dijet cross sections in e p collisions: Who is afraid of symmetric cuts?," submitted to Phys. Lett. B [hep-ph/0308116]
50. G. D'Agostini, Nucl. Instrum. Meth. A **362**, 487 (1995)
51. R. Engel, Z. Phys. C **66**, 203 (1995); R. Engel, J. Ranft, Phys. Rev. D **54**, 4244 (1996) [hep-ph/9509373]
52. J. Pumplin et al., JHEP **0207**, 012 (2002) [arXiv:hep-ph/0201195]
53. Z. Nagy, Z. Trocsanyi, Phys. Rev. Lett. **87**, 082001 (2001) [hep-ph/0104315]
54. C. Duprel et al., in "Monte Carlo Generators for HERA Physics" (Hamburg, Germany, 1999), A. Doyle, G. Grindhammer, G. Ingelman, H. Jung, Eds., p. 142, DESY-PROC-1999-02 [hep-ph/9910448]